energies

MDPI

Article

Neural Inverse Optimal Control of a Regenerative Braking System for Electric Vehicles

Jose A. Ruz-Hernandez [1,*], Larbi Djilali [1], Mario Antonio Ruz Canul [1], Moussa Boukhnifer [2] and Edgar N. Sanchez [3]

[1] Faculty of Engineering, Universidad Autonoma del Carmen, Campeche 24180, Campeche, Mexico
[2] Université de Lorraine, LCOMS, 57000 Metz, France
[3] Department of Electrical Engineering, Cinvestav Guadalajara, Av. del Bosque 1145, Col. El Bajío, Zapopan 45019, Jalisco, Mexico
* Correspondence:jruz@pampano.unacar.mx

Abstract: This paper presents the development of a neural inverse optimal control (NIOC) for a regenerative braking system installed in electric vehicles (EVs), which is composed of a main energy system (MES) including a storage system and an auxiliary energy system (AES). This last one is composed of a supercapacitor and a buck–boost converter. The AES aims to recover the energy generated during braking that the MES is incapable of saving and using later during the speed increase. To build up the NIOC, a neural identifier has been trained with an extended Kalman filter (EKF) to estimate the real dynamics of the buck–boost converter. The NIOC is implemented to regulate the voltage and current dynamics in the AES. For testing the drive system of the EV, a DC motor is considered where the speed is controlled using a PID controller to regulate the tracking source in the regenerative braking. Simulation results illustrate the efficiency of the proposed control scheme to track time-varying references of the AES voltage and current dynamics measured at the buck–boost converter and to guarantee the charging and discharging operation modes of the supercapacitor. In addition, it is demonstrated that the proposed control scheme enhances the EV storage system's efficacy and performance when the regenerative braking system is working. Furthermore, the mean squared error is calculated to prove and compare the proposed control scheme with the mean squared error for a PID controller.

Keywords: electric vehicles; regenerative braking; inverse optimal control; buck–boost converter; neural identifier

Citation: Ruz-Hernandez, J.A.; Djilali, L.; Ruz Canul, M.A.; Boukhnifer, M.; Sanchez, E.N. Neural Inverse Optimal Control of a Regenerative Braking System for Electric Vehicles. *Energies* **2022**, *15*, 8975. https://doi.org/10.3390/en15238975

Academic Editor: Joao L. Afonso

Received: 1 October 2022
Accepted: 18 November 2022
Published: 28 November 2022

1. Introduction

Electric vehicles (EVs) have demonstrated, in the present day, their importance in the solution of the environmental impact generated by conventional vehicles, such as air pollution and CO_2 emissions, and economic issues such as the gasoline prices [1]. The facility of using energy stored from the conversion of kinetic and potential energy into electrical energy only by changing the operation mode of an electrical motor to use it as a generator is one of the advantages of EVs that improve the driving performance and the life of the storage system [2]. One proposal to enhance EVs' driving range is the use of range extenders such as internal combustion engines, free-piston linear generator, fuel cells, micro gas turbines, and zinc–air batteries [3]. However, many disadvantages have been found such as the nonreduction of gas emission in some combinations, and the hard accessibility to some of the proposed range extenders. On the other hand, hybrid vehicles have been presented as an alternative to improve the performance of EVs by combining an internal combustion engine with an electric motor and reducing the emission of polluting gases [4]. Another proposed solution is the use of an external EV charger to administer energy to the battery bank. This type of EV is called a plug-in hybrid electric vehicle [5]. The operation of hybrid vehicles offers many advantages which also come with many challenges to ensure

the switching between both installed supply systems because of the combination of many technologies; as a result, these complex hybrid controllers are required [6]. The use of fully EV technology combining the main energy system (MES) and an auxiliary energy system (AES) can reduce the challenges described above [7]. The AES contains battery banks, supercapacitors, and power electronic devices, which improves the efficiency of these systems because of the latest advancements in MOSFETs [8].

In recent years, the regenerative braking capability in EVs has been one of the most important characteristics because it helps to improve the operation and efficacy of the regenerative braking system in electric vehicles [9]. As a result, numerous ideas have been put forth to achieve greater performance when operating EVs in a variety of scenarios where the main dynamics in storage systems are controlled. Due to the increasing production and demand of EVs on a global scale, studies have demonstrated that regenerative braking is an excellent strategy for energy conservation because it can retain any energy lost during an electric vehicle's braking.

Lately, many control strategies have been developed in different regenerative braking architectures. A case study created in [10] considered a unilateral boost operation connected to a DC motor and simulated the switched operation of the converter produced, which was mainly comprised of IGBT bridges. A Lyapunov stability analysis was applied to ensure the system's stability, and a proposed switching control law was implemented to achieve robust control.

In [11], a model predictive control was employed to manage the torque distributions, optimizing the hydraulic braking and motor torque, maximizing the regenerative braking system, and enhancing the energy storage system. This application of regenerative braking was explored with Simulink's AMESim software and was utilized to model the proposed control strategy and analyze various driving scenarios. Additionally, a real-time test was executed showing positive results.

The improvement of the driving range and battery extended life cycle was demonstrated in [12] using a regenerative braking architecture consisting of a three-phase induction motor powered by a DC–DC buck–boost converter connected in parallel with a lithium-ion battery and a supercapacitor, where the current dynamics of the regenerative braking mode were controlled by a PI controller. Additionally, a three-phase inverter and the braking forces produced by the traction on the EV's wheels were approximated using an artificial neural network (ANN).

In [13], to recover the energy wasted during the deceleration, a regenerative braking system composed of an ultracapacitor pack and battery was designed, obtaining an improvement in the efficiency of the regenerative braking in comparison with a standalone battery system because of the additional ultracapacitor pack. In [14], a PI controller was implemented with the same design as mentioned above to regulate the buck–boost converter output voltage. Using the exponential reaching law and a parameter optimization, a fuzzy logic sliding mode controller was implemented in [15] to keep the optimal slip value for an antilock braking system in an EV. Comparing the fuzzy sliding mode control in [15] and the fuzzy one in [16] with an intelligent sliding mode controller employed to track the desired slip during braking implemented in [17], the energy recuperation was improved considerably without overcharging the battery. Recently, nonlinear control algorithms, such as the inverse optimal, feedback linearization, and sliding mode, have been implemented in electrical drives, win systems, and biomedical applications among others.

In [18], inverse optimal control (IOC) was implemented to regulate the voltage of a DC–DC converter and compared with a PID controller under the same conditions resulting in better performance with the IOC. In [19], the same control scheme was proposed to ensure the tracking of the desired trajectory of an induction motor and to avoid the instability generated by disturbances. In [20], inverse optimal control was used in a feedback stochastic nonlinear system and it was proved that the asymptotic stability was guaranteed for the probability of control systems. However, the controllers previously mentioned require previous knowledge of the system parameters since the analysis of the control algorithms

is based on the mathematical models of the controlled system and these are not always easy to access in real operations. Additionally, their robustness and stability are not assured in the presence of disturbances [21].

The advances in technology create a need to solve problems presented in systems with complex, unknown dynamics, and highly coupled behavior. Engineers should make use of mathematical tools to solve these control problems. Neural networks are widely implemented to obtain a mathematical model approximating the unknown dynamics and use this information as the base to implement a conventional control algorithm. Different control problems have been resolved by using neural control such as in biomedical applications [22], microgrids [23], and in multiagent stabilization systems [24]. Nevertheless, this neural control is not widely implemented on regenerative braking systems for EVs [25].

This paper presents neural inverse optimal control (NIOC) for a regenerative braking system implemented in EVs. The proposed controller is used to regulate the current and voltage of the buck–boost converter related to the AES to recover the wasted energy during braking and enhance the MES's efficiency. The main contributions of the present paper are: (1) An online-identification-based recurrent high order neural network (RHONN) trained by an extended kalman filter (EKF) as a build-up to approximate the DC buck–boost behaviors. (2) Based on the obtained neural model, the inverse optimal control strategy is synthesized and implemented to track the buck–boost current and voltage desired dynamics. (3) Since the proposed controller is based on a neural identifier, robustness to parameter variations and disturbances is ensured. (4) To verify stability and robustness of the proposed control scheme, a comparison with the conventional PID controller is implemented. (5) By the implementation of the proposed controller for the AES, the storage of energy in the MES has more efficiency, and the loss of energy is largely reduced in comparison with a standalone MES.

The rest of the paper is organized as follows: In Section 2, the material and methods used in the article are described and the steps followed to structure this paper are briefly explained to get the major idea and process of this work. In Section 3, the regenerative braking problem is described. In addition, the buck and boost operation of the buck–boost converter is explained. In Section 4, mathematical preliminaries are introduced where the fundamentals of the corresponding equations used to develop the system identification and proposed control scheme for the regenerative braking system are presented. In Section 5, the buck–boost converter system modeling, and DC motor mathematical modeling are described. In Section 6, the neural controller design is presented. Additionally, the design of the reference generator and the DC motor control equations are presented. Section 7 illustrates the simulation results for the different steps implemented in the article where the validation of the neural controller with and without the regenerative braking system is shown. Furthermore, the robustness test is implemented where the results are compared with a PID controller and illustrated not only graphically but with results obtained from the mean squared error. Finally, Section 8 is the conclusion of the article where the obtained results are discussed and future work is proposed.

2. Materials and Methods

The method used to achieve the results obtained in this article follows the next steps:

- The goal of this article is to improve the regenerative braking system of an electric vehicle. The element of that system that allows the control of the current and voltage variables is the buck–boost converter. The validation and simulation of the proposed controller and regenerative braking system are implemented using the SimPower System toolbox of Matlab (Matlab, Simulink. de 1994–2022, ©The Math Works, Inc.).
- A mathematical model of the buck–boost converter [26] is used to develop the RHONN equations as in [27].
- After the RHONN equations are acquired, the extended Kalman filter is used to train the identifier and estimate the values of the dynamics in the buck–boost converter. The validation is illustrated in Figures 1 and 2.

- The trained RHONN allows the design of the neural controller. In our case, it is a neural inverse optimal controller.
- The validation of the proposed control scheme is to track the proposed time-varying trajectories without connecting the complete regenerative braking system. These results are illustrated in Figures 3–5.
- After the control scheme is validated, the design of a reference generator is developed. This reference generator provides the value in volts within which the buck–boost converter must operate during a driving operation. This signal is generated through the motor's DC dynamics, which are regulated using a PID controller.
- Once the whole regenerative braking system is connected (battery bank, supercapacitor and buck–boost converter, DC motor, etc.) the correct operation of the regenerative braking system is validated.
- From this validation the controlled variables, the better performance in the state of charge of the battery bank, and the correct operation of the supercapacitor charge and discharge operation modes are illustrated in Figures 6–11.
- Lastly, the robustness test is implemented by comparing the performance of the controller with a classic PID controller. In addition, not only the graphic results are demonstrated in Figures 11–13 but the mean squared error is calculated to validate the result obtained.

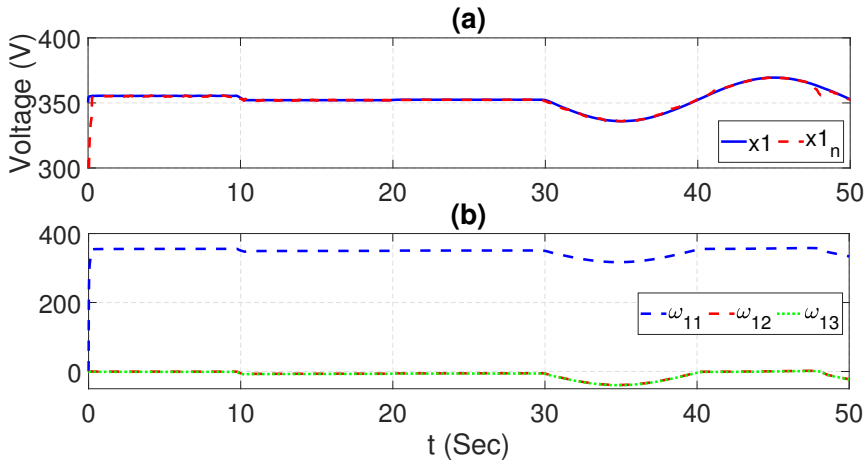

Figure 1. Voltage identification (**a**) and NN's weights (**b**).

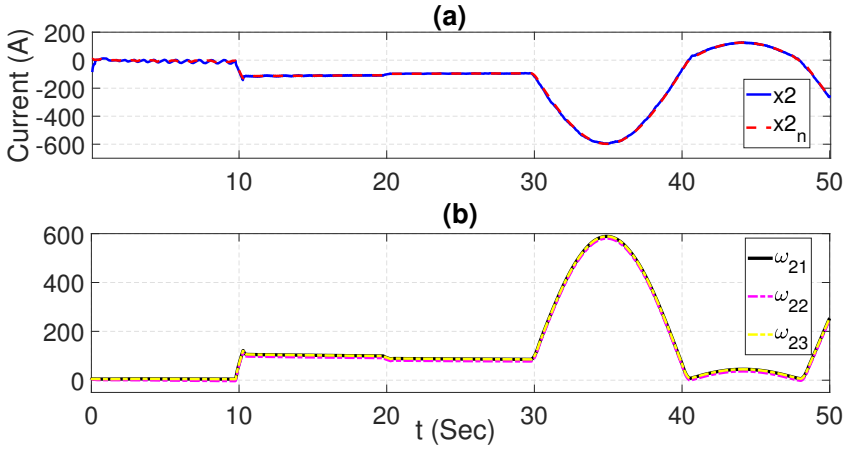

Figure 2. Current identification (**a**) and NN's weights (**b**).

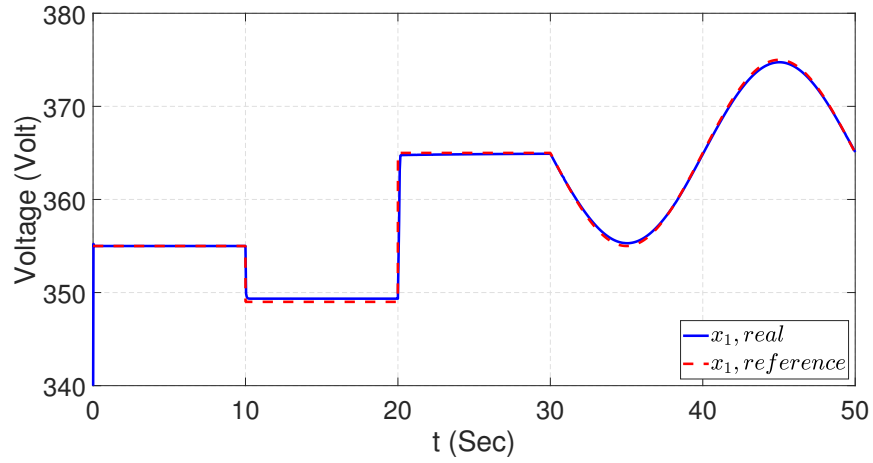

Figure 3. AES voltage trajectory tracking.

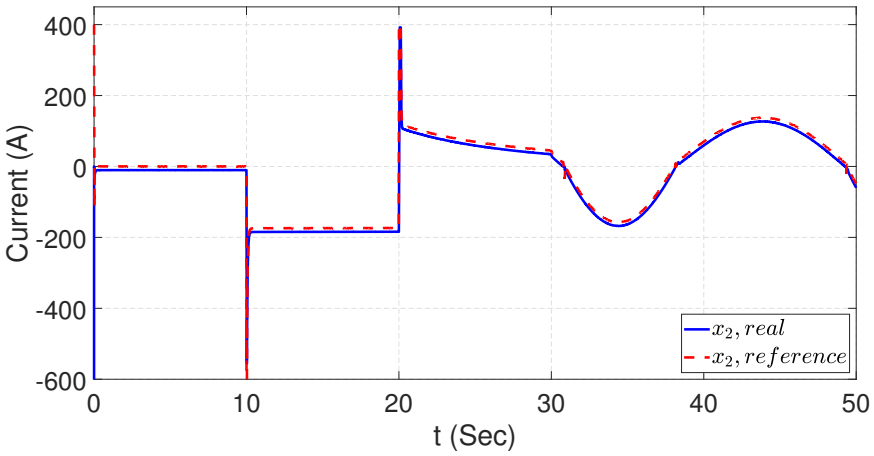

Figure 4. AES current trajectory tracking.

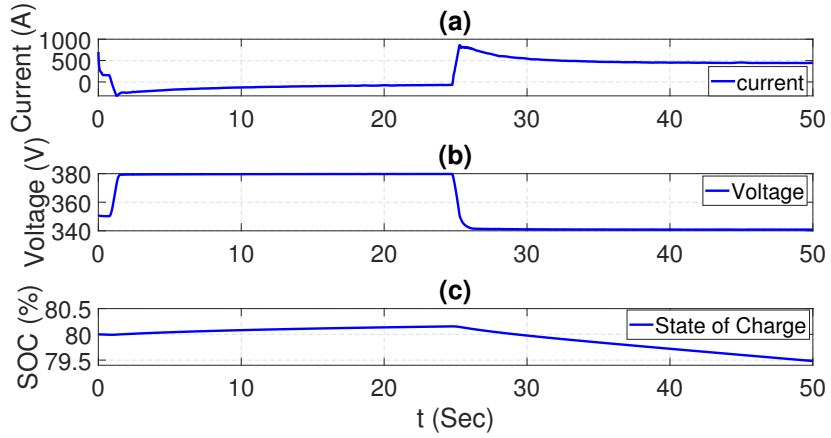

Figure 5. AES charging during trajectory tracking. (**a**) Illustrate the obtained current during the tracking operation, (**b**) the obtained voltage during the tracking operation and (**c**) the state of charge of the supercapacitor during the tracking operation. and discharging.

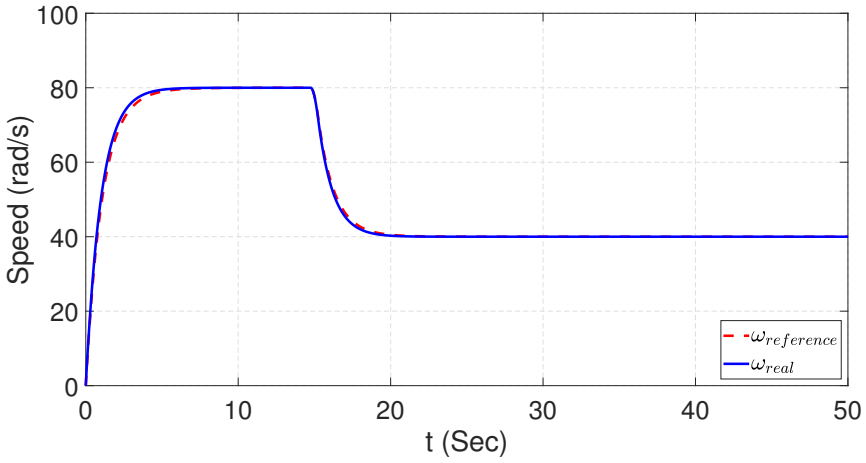

Figure 6. Motor speed control.

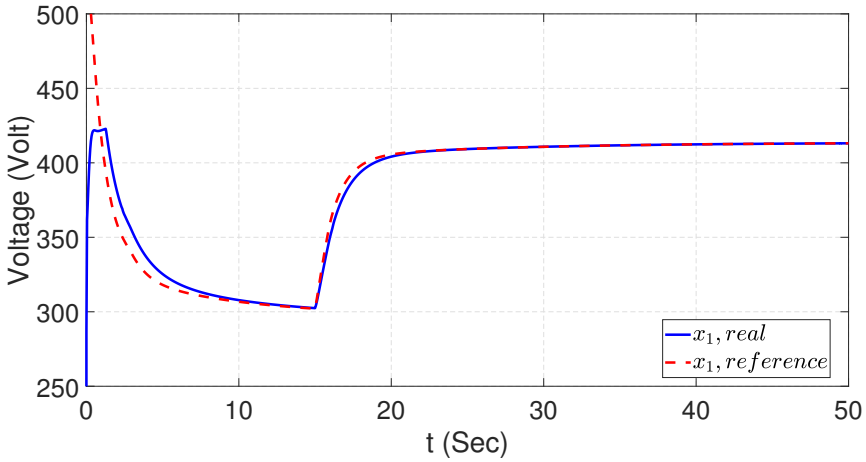

Figure 7. AES voltage control during regenerative braking.

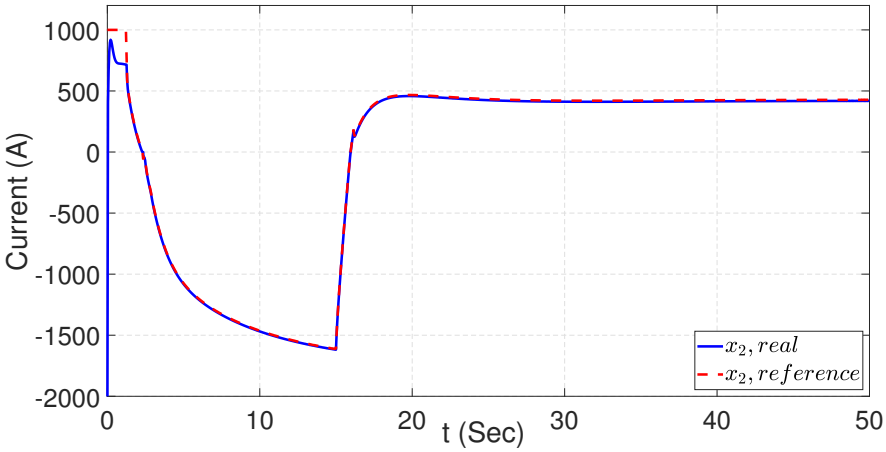

Figure 8. AES current control during regenerative braking.

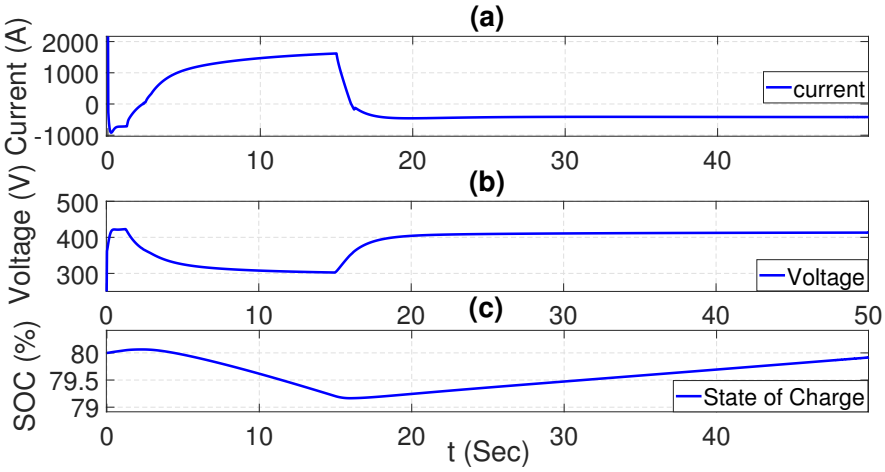

Figure 9. AES supercapacitor SOC. (**a**) Illustrate the obtained current during the vehicle operation, (**b**) the obtained voltage during the vehicle operation and (**c**) the state of charge of the supercapacitor during the operation.

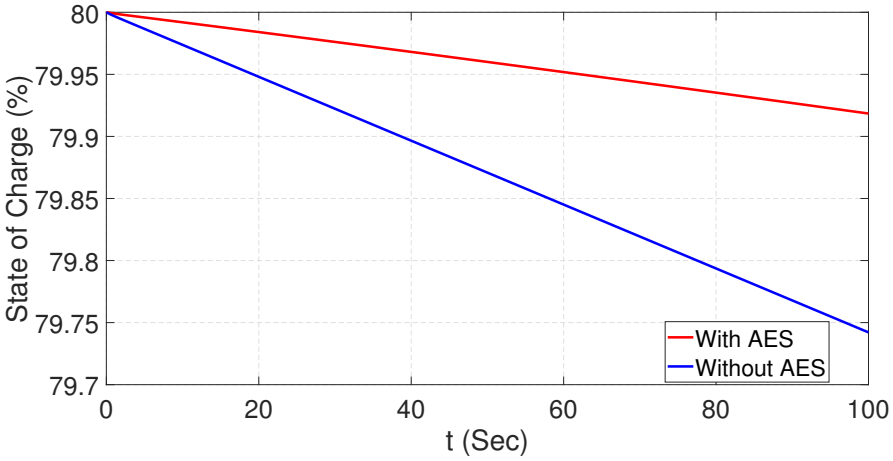

Figure 10. MES battery bank SOC comparison with and without AES.

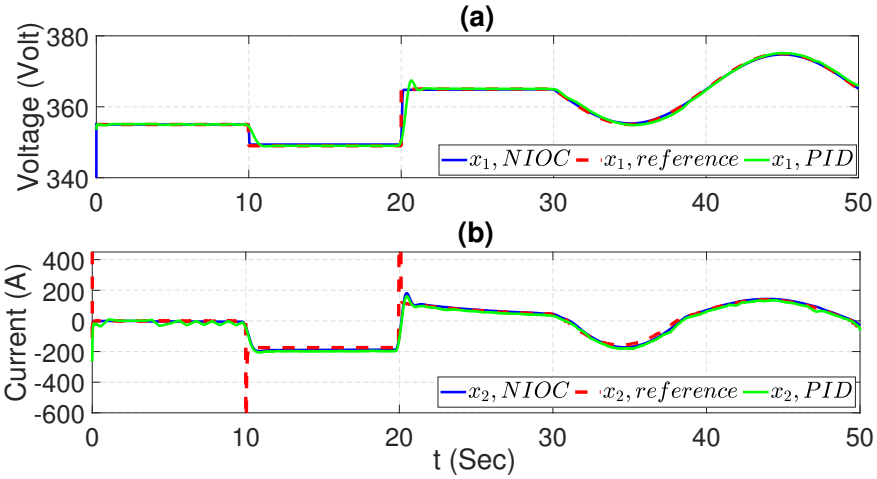

Figure 11. Influence of R changes on PI and NIOC: (**a**) voltage, (**b**) current.

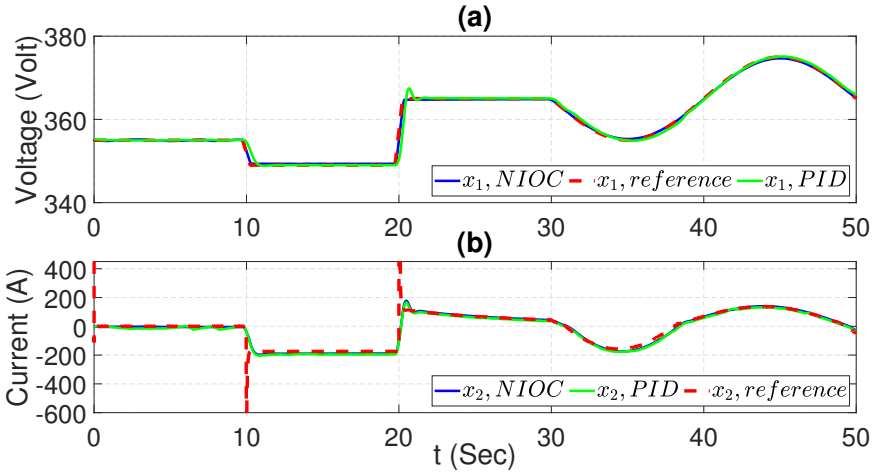

Figure 12. Influence of L changes on PI and NIOC: (**a**) voltage, (**b**) current.

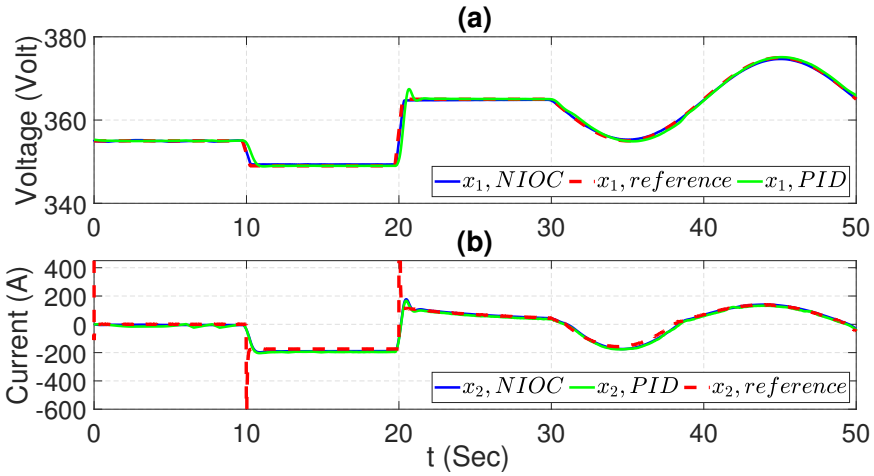

Figure 13. Influence of C changes on PI and NIOC: (**a**) voltage, (**b**) current.

3. Regenerative Braking Description

A regenerative braking system as depicted in Figure 14 allows the recovery of kinetic energy produced during braking and its utilization to improve the energy storage efficiency and extend the operating distance of the EV [2]. This system is composed of a supercapacitor and buck–boost converter, which are part of the AES. In addition, a battery bank is used to administer the energy to the electrical motor contained in the MES. The supercapacitor and the buck–boost converter are connected as illustrated in Figure 15, with the objective of increasing or decreasing the output voltage depending on the following operation modes.

Buck operation: In this mode, the output voltage is decreased regarding the input voltage. To achieve this, T1 is off and T2 is activated, then, the energy is transferred from the capacitor (V_c) to the supercapacitor voltage (V_{sc}). At the moment T2 is turned on, current flows from the capacitor C, generating current I_c to the supercapacitor. As a result, a fraction of this energy is charged into inductance L. On the other hand, when T2 is turned off, the current charged in L is discharged into V_c through diode D1, driving the current in the direction of capacitor C [14].

Boost operation: On the other hand, in this mode, the output voltage is increased. To do so, T2 is deactivated and T1 is activated to transfer energy from supercapacitor Vsc to battery bank Vc. When T1 is on, the energy is acquired from the capacitor, and stored in inductance L. Reversely, when T1 is OFF, the energy stored in the inductance is transferred into the capacitor through diode D2, and kept in the battery bank.

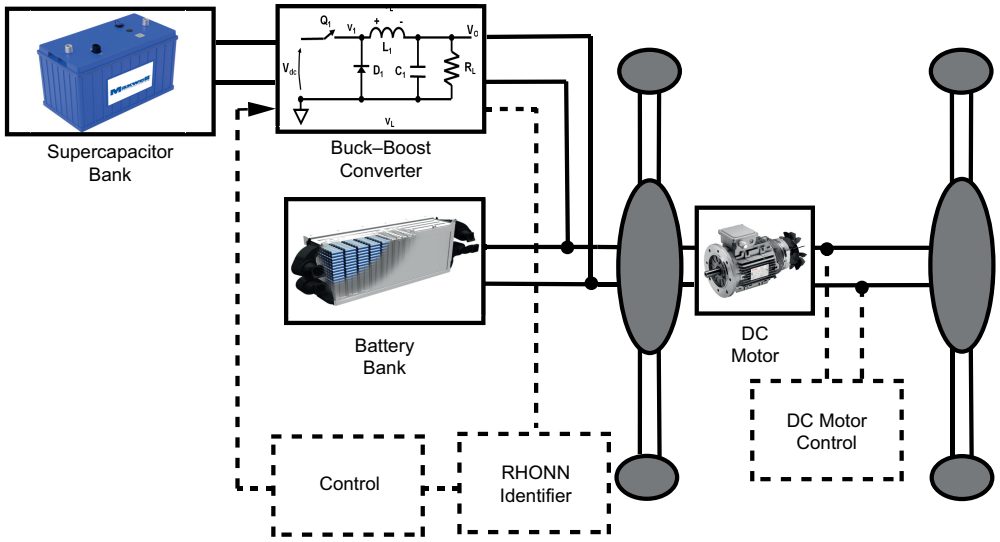

Figure 14. Regenerative braking system topology.

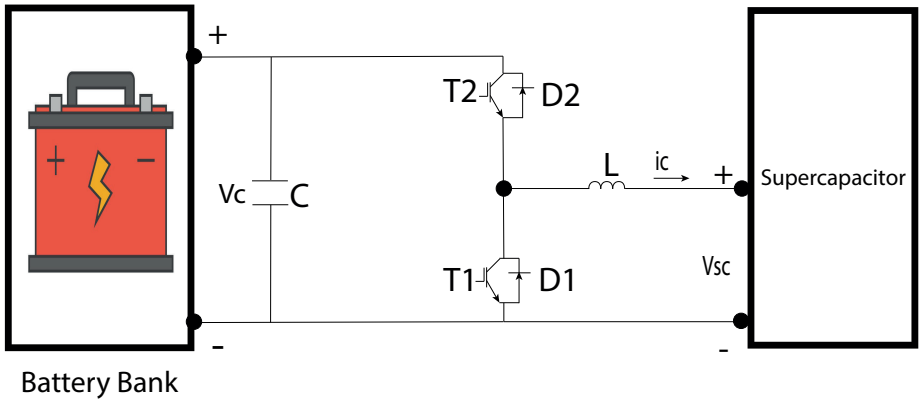

Figure 15. Buck–boost converter topology.

During the braking operation, the brake manages the electricity generated by the motor into the batteries or capacitors. The DC–DC converter operates in boost function during acceleration while it operates into buck function in deceleration, which makes it easier to charge up the supercapacitor.

4. Mathematical Preliminaries

4.1. Discrete-Time Inverse Optimal Control

Consider the following perturbed discrete-time nonlinear system [28]

$$x_{k+1} = f(x_k, k) + B(x_k)u(x_k, k) + d(x_k) \tag{1}$$

$$y_k = h(x_k) \tag{2}$$

with x_k the state variable, u_k the input vector, y_k the output vector to be controlled, $f(x_k)$, $B(x_k)$, and $h(x_k)$ smooth and bounded vectors. Considering y_k contains the full state vector, the objective is to force the controlled dynamics to track selected trajectories, then the tracking error is as follows

$$e_{k+1} = x_{k+1} - x_{ref,k+1} \tag{3}$$

with $x_{ref,k}$ the desired trajectory vector. The error dynamics at $k+1$ is expressed by

$$e_{k+1} = f(x_k, k) + B(x_k)u(x_k, k) + d(x_k) - x_{ref,k+1} \tag{4}$$

For the optimal problem solution, the cost function is minimized by solving the Hamilton–Jacobi–Bellman (HJB) partial differential equation (PDE). However, in some cases the solution of these classes of equations is difficult to obtain [29]. For the tracking trajectory, the cost function of system (4) is selected as

$$J(e_k) = \sum_{k=0}^{\infty} (l(e_k) + u - k^T R u_k) \tag{5}$$

where J: $\Re^n \rightarrow \Re^+$ is a performance measure, l: $\Re^n \rightarrow \Re^+$ is a positive semidefinite function, and R: $\Re^n \rightarrow \Re^{n \times m}$ is a positive real symmetric matrix. When the cost function J is optimal, it is noted as $J*$ and it is defined as Lyapunov function $V(e_k)$, which is time-invariant and should satisfy the discrete-time Bellman equation defined as follows

$$V(e_k) = \min_{u_k} l(e_k) + u_k^T R(e_k) u_k + V(e_{k+1}) \tag{6}$$

Hence, the discrete-time Hamiltonian equation is expressed as follows

$$H(e_k, u_k) = l(e_k) + u_k^T R(e_k) u_k + V(e_{k+1}) - V(e_k) \tag{7}$$

The optimal control law is obtained using $H(e_k, u_k) = 0$, and the gradient of (7)'s right-hand side is calculated with respect to u_k [28], then

$$u_k^* = -\frac{1}{2} R(e_k)^{-1} B(x_k)^T \frac{\partial V(e_{k+1})}{\partial e_{k+1}} \tag{8}$$

where $V(0) = 0$ is the boundary condition of $V(e_k)$ which should be satisfied and u_k* is the optimal control law. Using (8) in (6), the discrete-time HJB equation is

$$V(e_k) = \frac{1}{4} \frac{\partial V^T(e_{k+1})}{\partial e_{k+1}} R(e_k)^{-1} B(x_k)^T \frac{\partial V(e_{k+1})}{\partial e_{k+1}} + l(e_k) + V(e_{k+1}) \tag{9}$$

Determining the solution of the HJB PDE (9) for $V(e_k)$ is not trivial. To do so, the discrete-time inverse optimal control (IOC) technique and a Lyapunov function are used to synthesize the respective control law [29,30]. To state the above problem as an IOC one, the following definition is established.

Definition 1 ([28]). *For system* (1)*, the control law in* (8) *is considered to be IOC (globally) stabilizing if:*

(1) It ensures that (8) *has (global) asymptotic stability for* $e_k = 0$*;*
(2) It minimizes the cost function (5) *for which* $V(e_k)$ *is positive definite function such that*

$$\overline{V} := V(e_{k+1}) - V(e_k) + u_k^* B(x_k) u_k^* \leq 0. \tag{10}$$

Thus, the IOC synthesis is based on $V(e_k)$ from the previous definition. Then,

Definition 2 ([28]). *Let us select* $V(x_k)$*, which is established to be a radially bounded positive definite function such that for each* x_k *there exist* u_k *and*

$$\Delta V(e_k, u_k) < 0 \tag{11}$$

where $V(e_k)$ *is a discrete-time control Lyapunov function (CLF), which should be defined to satisfy conditions (1) and (2) of Definition 1. Thus, the CLF is selected as follows*

$$V(e_k) = \frac{1}{2} e_k^T P(e_k) \tag{12}$$

with $P \in \Re^{n\times n}$ and $P = P^T > 0$. By selecting an appropriate matrix P, the control signal (8) guarantees the equilibrium point $e_k = 0$ of (4)'s stability. Additionally, the control law (8) with (12), which is considered as an inverse optimal control law for (1), optimizes the meaningful cost function in (5). Moreover, by using (8) in (12), the IOC law is established as follows:

$$u_k^* = \frac{1}{2}\left(R + \frac{1}{2}B(x_k)^T P B(x_k)\right)^{-1} B(x_k)^T P(f(x_k) - x_{ref,k+1}) \tag{13}$$

where P and R are positive definite matrices. Details about the NIOC synthesis is explained in [28]. To achieve adequate performance of the discrete-time IOC scheme, a priori knowledge of the model parameters is requested, which is not always fulfilled in real-time applications. In addition, since this control scheme is based on a mathematical model, robustness to parameters variations and disturbances cannot be ensured. To improve it, an RHONN identifier trained online with an EKF is proposed.

4.2. Discrete-Time Recurrent High-Order Neural Networks

In these last years, recurrent neural networks have been implemented to identify and approximate the mathematical models of complex systems [21]. The RHONN has demonstrated that is a good choice in nonlinear system identification, which consists of adjusting the parameters of an appropriately selected model according to an adaptive law. Using a series–parallel configuration, the estimated state variable of a nonlinear system using an RHONN identifier is given by [27]

$$\chi_{i,k+1} = \omega_i^T \phi_i(x_k) + \overline{\omega}_i^T \varphi_i(x_k, u_k) \tag{14}$$

where $\chi_{i,k+1}$ is the state of the i^{th} neuron which identifies the i^{th} component of x_k, $x_k = [x_{1,k}, ..., x_{n,k}]$ is the state vector, $\omega_{i,k} \in \Re^{L_i}$ are the adjustable synaptic weights of the NN, $\omega_{i,k}$ represent the adjustable weights, and $\overline{\omega}_{i,k}$ are the fixed weights, φ_i is a linear function of the state vector or vector input u_k depending to the system structure or external inputs to the RHONN model, and $u \in \Re^m$ $u = [u_{1.k}, u_{2,k}, \ldots, u_{m,k}^T]$ is the input vector to the network. The function $S(.)$ is a hyperbolic tangent function defined as

$$S(x_k) = \alpha_i \tanh(\beta_i x_k) \tag{15}$$

where x_k is the state variable; α and β are positive constants. Figure 16 illustrates the i^{th} RHONN identifier scheme.

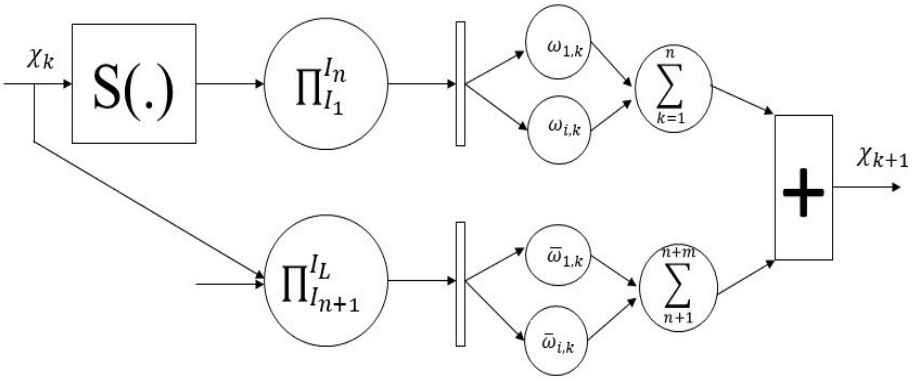

Figure 16. RHONN identifier scheme.

To train the proposed RHONN identifier, an EKF is used. The algorithm model is defined as follows

$$w_{i,k+1} = w_{i,k} + \eta_i K_{i,k} e_{i,k} \quad (16)$$
$$K_{i,k} = P_{i,k} H_{i,k} M_{i,k} \quad (17)$$
$$P_{i,k+1} = P_{i,k} - K_{i,k} H_{i,k}^T P_{i,k} + Q_{i,k} \quad (18)$$
$$e_{i,k} = x_{i,k} - \chi_{i,k} \quad i = 1, 2, \cdots, n \quad (19)$$
$$M_{i,k} = \left[R_{i,k} + H_{i,k}^T P_{i,k} H_{i,k} \right]^{-1} \quad (20)$$

with $e_i \in \mathbb{R}$ the identification error to be minimized, η_i a training algorithm design parameter, $K_{i,k} \in \mathbb{R}^{L_i \times m}$ the Kalman matrix, $Q_{i,k} \in \mathbb{R}^{L_i \times L_i}$ and $R_{i,k} \in \mathbb{R}^{m \times m}$ positive definite constant matrices, $P_i \in \mathbb{R}^{L_i \times L_i}$ an adjustable diagonal matrix, and $H_i \in \mathbb{R}^{L_i \times m}$ an adjustable matrix defined as the state derivative with respect to the neural identifier's adjustable weights. Details of the RHONN identifier and the respective EKF training algorithm, including a stability proof is explained in [21,31].

5. System Modeling and Neural Control

5.1. Buck–Boost Model

The used DC–DC converter in this application was composed of boost and buck converters. The first one is used under charge conditions while the second one is used under discharge conditions. The boost converter model is defined as [26]

$$x_{1,k} = (1 - \frac{ts}{RC}) x_{1,k} - \frac{ts}{c} x_{2,k} \quad (21)$$
$$x_{2,k} = x_{2,k} + \frac{ts}{L} U_{btt} u_c \quad (22)$$

The buck converter model is given by [26]

$$x_{1,k} = (1 - \frac{ts}{RC}) x_{1,k} + \frac{ts}{c} x_{2,k} \quad (23)$$
$$x_{2,k} = x_{2,k} + \frac{ts}{L} U_{btt} u_c \quad (24)$$

where $x_{1,k}$ is the converter output voltage, $x_{2,k}$ is the output current, U_{btt} is the battery voltage, u_c is the input vector, L is the inductance (H), R is the load resistance (Ω), C is the capacitor (F), and t_s is the sample time.

5.2. DC Motor

To illustrate the performance of the regenerative braking and for system completeness, a DC Motor was used as a drive system of the EV [14]. The DC machine's dynamics are governed by two attached first-order equations concerning the armature current and angular velocity as in [32]. The mathematical model is defined by [32]:

$$L \frac{di}{dt} = u - Ri - \lambda_0 \quad (25)$$
$$J \frac{d\omega}{dt} = k_t i - \tau_l \quad (26)$$

where i is the armature current (A), u is the terminal voltage (V), ω is the angular velocity (rad/s), J is the inertia of the motor rotor and load (kg m^2), R is the armature resistance (ω), L is the armature inductance (H), λ_0 is the back electromotive force (EMF) constant, k_t is the torque constant, and τ_l is the load torque.

6. Neural Controller Design

To approximate the used buck–boost power converter's dynamics, an RHONN identifier trained online by an EKF was employed, then based on the obtained model, the IOC was synthesized to manage the current flow and ensure the charging and discharging operating modes of the AES. Due to the similarity between the buck and boost converter models and the adaptive nature of the RHONN, a single neural identifier is proposed for both cases as follows

$$\begin{aligned} \hat{x}_{1,k} &= \omega_{1,1}(k)S(x_1) + \omega_{1,2}(k)S(x_2) \\ &+ w_{1,3}S(x_1)S(x_2) + \varpi_1 x_2 \end{aligned} \tag{27}$$

$$\begin{aligned} \hat{x}_{2,k} &= \omega_{2,1}(k)S(x_2) + \omega_{2,2}(k)S(x_1) \\ &+ w_{2,3}S(x_1)S(x_2) \end{aligned} \tag{28}$$

Using the compact form, (27) and (28) can be rewritten as follows

$$\hat{x}_{k+1} = \hat{F}(x_k) + \hat{B}u_k^* \tag{29}$$

$$\hat{y}_k = x_{2,k} \tag{30}$$

where $[\hat{x}_{1,k+1}, \hat{x}_{2,k+1}]^T$ are the estimated dynamics of $[x_{1,k}, x_{2,k}]^T$, u_k is the input signal, $\hat{y}_k$ is the output to be tracked, and $\hat{B}$ is the control matrix defined as $\hat{B} = diag[0, \varpi_2]$. For the controller design, the proposed controller was carried out for the current trajectory tracking. The current tracking error at $k+1$ was obtained as

$$\begin{aligned} \hat{e}_{k+1} &= \omega_{2,1}(k)S(x_2) + \omega_{2,2}(k)S(x_1) \\ &+ w_{2,3}S(x_1)S(x_2)\varpi_2 u_k - x_{ref,k+1} \end{aligned} \tag{31}$$

Then, the equivalent NIOC was calculated using the same steps as in Section 4.1 as follows

$$u_k^* = \frac{1}{2}\left(R + \frac{1}{2}B(x_{2,k})^T P B(x_{2,k})\right)^{-1} B(x_{2,k})^T P e_{k+1} \tag{32}$$

where P and R are positive definite matrices.

Reference Generator Development

To define the buck–boost current desired value, a current reference generator was developed. The charge reference was defined as the energy contained in the supercapacitor as a function of the energy generated by the DC motor. Considering the work and energy theorem "**the work done between point A and point B on a particle results on the increase of its kinetic energy**" cited in [33], the following expression can be written

$$W_{A\to B} = \int_A^B P d_t \tag{33}$$

Using the work and energy theorem on the DC motor, the energy can be estimated for an interval time $t \in [k\delta, (k+1)\delta)]$ as [14]

$$E(t) = \int_{k\delta}^{t} P_k d\xi + E_k \tag{34}$$

where the DC motor power can be estimated as $P = \tau_e \omega$. The energy in the supercapacitors during the charging mode can be estimated as

$$E_C^{ref-c}(t) = -k_p \int_{k\delta}^{t} sat_1(P) d\xi + E_{ck} \tag{35}$$

and during the discharging mode, it can be given as

$$E_C^{ref-d}(t) = k_p \int_{k\delta}^{t} sat_2(P)d\xi + E_{ck} \tag{36}$$

with $E_C^{ref-c}(t)$, $E_C^{ref-d}(t)$ and $0 < k_p < 1$ as the charge reference, discharge reference, and a constant representing the lost energy during transformation, respectively. sat_1 represent a saturation function in the range of $(-\infty, 0)$ and sat_2 the same function in the range of $(0, \infty)$. The energy reference for the supercapacitor is estimated as the sum result of both references.

$$E_C^{ref} = E_C^{ref-c} + E_C^{ref-d} \tag{37}$$

Then, the buck–boost voltage reference can be obtained using the last supercapacitor energy equation resolved for the voltage

$$V_{cr} = \sqrt{\frac{2E_C}{C}} \tag{38}$$

where V_{cr} is the reference voltage in the supercapacitor, E_c is the energy stored, and C is the capacitance.

To track the buck–boost voltage, the NIOC scheme was applied. Using (27), the voltage error at $k+1$, evc_{k+1} was calculated as follows

$$\begin{aligned} e_{Vcr,k+1} &= \omega_{1,1}(k)S(x_1) + \omega_{1,2}(k)S(x_2) \\ &+ w_{1,3}S(x_1)S(x_2) + \omega_1 x_2 - V_{cr} \end{aligned} \tag{39}$$

Then, the NIOC was applied to determine the buck–boost current reference for the supercapacitor as follows

$$i_{cr} = \frac{1}{2}\left(R + \frac{1}{2}B(x_{1,k})^T P B(x_{1,k})\right)^{-1} B(x_{1,k})^T P e_{Vcr,k+1} \tag{40}$$

The control scheme for the regenerative braking system using NIOC and the current reference generator is illustrated in Figure 17.

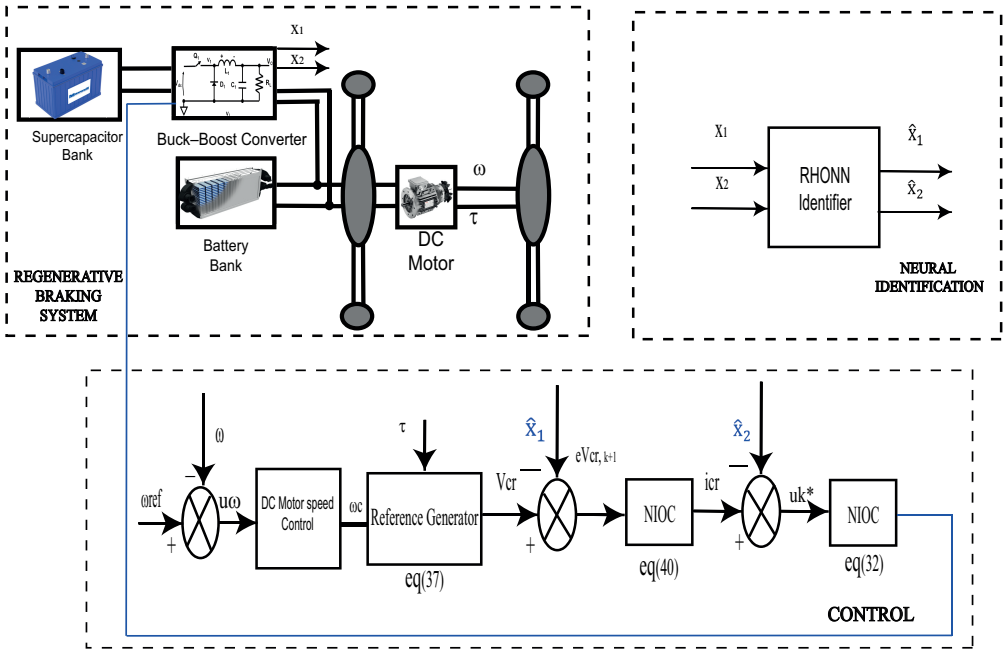

Figure 17. Regenerative braking system control scheme.

The DC motor speed was controlled using a PI controller to track a desired reference

$$u_{\omega} = k_{\omega_l p}(\omega_{l,ref} - \omega_l) + k_{\omega_l i}\int_0^t (\omega_{l,ref} - \omega_l) \tag{41}$$

where $\omega_{l,ref}$ is the motor reference speed and $k_{\omega_l p}$ and $k_{\omega_l i}$ are proportional and integral controller gains, respectively.

7. Simulation Results

The proposed control scheme as well as the respective MES and AES were implemented and evaluated using the SimPower System toolbox of Matlab (Matlab, Simulink. de 1994–2022, ©The Math Works, Inc.). The parameters of the AES and MES are listed in Table 1.

Table 1. Parameters of the AES and MES.

Description	Unit
Converter resistance R.	50 Ω
Converter inductance L	13×10^{-3} H
Converter capacitance C_1	2×10^{-3} F
Converter capacitance C_2	1×10^{-6} F
Supercapacitor voltage V_{sc}	350 V
Battery bank voltage V_c	500 V
Initial SOC	80%
Sampling time (t_s)	1×10^{-5} s

7.1. Neural Identification

The realized RHONN identification allowed us to obtain a satisfactory estimation of the system states, which were, in this case, the voltage x_1, k and the current x_2, k during different operation modes. Figure 1 demonstrates the neural identification of the voltage (x_1, k) and its respective neural weights' changes during the operation of the time-varying signals.

Figure 2 presents the neural identification of the current (x_2, k) and its respective neural weights' dynamics that adjust over the operation with the time-varying trajectories.

From the obtained results, it is clear that the proposed RHONN identifiers successfully approximated the voltage and the current dynamics of the AES, even though time-varying trajectories were applied. In addition, all neural weights were bounded. This allowed a correct operation for the recognition of the dynamics of the buck–boost converter because the capability of identifying these variables over time-varying signals let the system operate in different conditions. Furthermore, the implementation of the neural controller did not represent a problem, with the neural identifier working correctly.

7.2. Buck–Boost Trajectories Tracking

In this test, the objective was to demonstrate the trajectories tracking of the AES voltage and current to validate the correct operation of the proposed NIOC scheme. A trajectory was proposed to show the dynamics regulation without connecting the whole regenerative braking system.

The proposed trajectory to be tracked was a time-varying signal, whose amplitude was changed between 340 V and 360 V. Figure 3 presents the obtained results for the voltage (x_1, k) at the output of the buck–boost converter used in the AES system controlled by the proposed NIOC scheme. As is shown, the tracking made by the controller operated correctly and followed the variations of the signal.

Figure 4 demonstrates the behavior of the current (x_2, k), as measured at the inductance of the buck–boost converter. As a result of the good performance of the neural controller for the voltage (x_1, k), the regulation and tracking of the current dynamics worked correctly.

Figure 5a–c display the current, voltage, and state of charge (SOC) of the AES, respectively. Different voltage values were applied to verify the charging and discharging operations of the AES. The voltage had an initial value of 380 V where the buck mode was activated and the supercapacitor was charging. Then, at 25 s, the voltage value was modified to 340 V resulting in the boost mode turning on and the supercapacitor discharging. The conclusion obtained with the voltage values was that the supercapacitor had the capacity to work over charging and discharging operations, which helped extend the life cycle and SOC of the battery when the whole system was connected.

From the obtained results, it is clear that the proposed control scheme (NIOC) ensured the tracking of the proposed trajectories for both the voltage and current of the AES. In addition, the charging and discharging operation modes of the AES were achieved.

7.3. Regenerative Braking System Trajectories Tracking

The objective of this section was to test the complete system functionality including the AES, MES, and the DC motor installed on the EV. The trajectories to be tracked were calculated using the reference generative block (38) where the motor speed was the input and the voltage reference (V_{cr}) was the output. This voltage output was used in the control loop of the AES where a cascade-controller-based NIOC scheme was used to regulate the voltage and the current of the buck–boost converter, respectively, with the objective to ensure the charge and discharge of the AES supercapacitor. The speed of the DC motor was controlled by a PI controller where a time-varying trajectory was tracked as presented in Figure 6.

Figure 7 presents the voltage's desired trajectory tracking, obtained from the reference generator block (38), using NIOC when the EV was fully operated. During acceleration, the voltage value decreased toward 340 V, the boost mode was activated, and the supercapacitor was discharging, allowing the AES's participation in the total EV's needed energy; as a result, the MES's charge duration was enhanced. However, during deceleration the voltage value increased to reach 350 V, the buck mode was turned on, and the supercapacitor was charging, which helped to recuperate the EV energy waste.

Figure 8 illustrates the current trajectory tracking using the proposed NIOC during the regenerative braking, where the reference trajectory was obtained from the NIOC voltage controller.

Figure 10 displays the SOC behavior of the MES battery bank without (blue) and with (red) the AES during the operation of the regenerative braking system. This demonstrated the enhancement of the battery operation using the regenerative braking system. The results obtained showed that the battery SOC decreased slowly with the AES in comparison to when the AES was not implemented.

The SOC of the AES as well the supercapacitor voltage and current are presented in Figure 9, where the supercapacitor is discharging when the EV is in an acceleration state and charging otherwise.

As results of this experiment, the proposed control scheme ensured the trajectory tracking of the AES voltage obtained from the reference regenerative block. The voltage value was automatically changed according to the acceleration or deceleration of the motor EV. In addition, the proposed controller achieved an adequate trajectory tracking of the AES current. On the other hand, the SOC of the MES was largely improved by using the proposed AES control methodology, which helped to recuperate the energy during deceleration and enhance the MES's charge duration. This demonstrated that the regenerative braking system had a good performance and operation when implementing the complete scheme as illustrated in Figure 17. However, it is necessary to add another test to prove even further the good operation of the EV architecture proposed in this article.

7.4. Robustness Test

In this test, the AES parameters were changed to examine the robustness of the proposed NIOC. In addition, a comparison with the classical PI controller was done to

illustrate the potential of the proposed neural control scheme. The obtained results of the AES when varying the parameters are presented in Figures 11–13.

The goal of this test was to vary the nominal values of the components that integrate the AES parameters described before in Table 1 and demonstrate the capability of the neural controller to operate over changes in their conditions, which could be considered as parasitic signals that were not part of an ideal electric vehicle's system. Figure 11 illustrates the voltage and current trajectories tracking of the AES when resistor R was changed by 200% of its nominal value.

Figure 12 demonstrates the voltage and current trajectories tracking of the AES when inductance L was changed by 100% of its nominal value.

Figure 13 demonstrates the voltage and current trajectories tracking of the AES when resistor C was changed by 70% of its nominal value.

From the simulation results, we can observe that parameter variations had an important impact on the AES voltage and current controlled by the PI controller, with a high coupling between the control axes and a sluggish response time. However, the proposed controller (NIOC) ensured an adequate performance in the presence of parameter variations, the decoupling was ensured, and the response time was improved compared with that of the PI controller. From this test, we can consider that the proposed controller had better performance and was robust to AES parameter variations and these results were supported by the mean squared error calculated to validate the statement made with these results. Table 2 illustrates the results for the voltage control robustness test while Table 3 describes the mean squared error for the current dynamics. One of the disadvantages of the PID controller was its capacity to reach the trajectory desired, which meant the squared error was farther from zero in comparison with that of the NIOC.

Table 2. Mean squared error in x_1.

Mean Squared Error of Tracking Trajectories in x_1	
Controller	**Mean Value**
PID	16.026×10^{-11}
NIOC	4.8822×10^{-11}

Table 3. Mean squared error in x_2.

Mean Squared Error of Tracking Trajectories in x_2	
Controller	**Mean Value**
PID	140.290×10^{-9}
NIOC	2.2314×10^{-9}

8. Conclusions

This article presented a regenerative braking system for electrical vehicles controlled by a neural inverse optimal controller. The control scheme was used to regulate the dynamics of the AES composed of a buck–boost converter and a supercapacitor, with the objective to enhance the energy recovery during braking and to participate in the delivered MES's energy during acceleration. The proposed controller was developed using a recurrent high-order neural network identifier, and online training by the extended Kalman filter based algorithm, which allowed us to approximate the AES's behavior during the different operation modes. The validation of the correct identification of the dynamics with the RHONN was illustrated correctly with the results obtained in the simulation. This responded to one of the statements mentioned about the implementation and correct operation of recurrent high-order neural networks in nonlinear systems.

The neural controller test with the proposed time-varying trajectories helped to achieve the correct implementation and operation of the dynamics before the complete system was connected. This was considered because working with the complete regenerative braking system before the tuning of the controllers may present some issues that could easily be solved by analyzing the controller separately first. The controller was used to track the desired trajectories of the AES voltage and current, where a reference generator block was utilized to define the voltage's desired value considering the electrical vehicle operation modes. This reference generator block was very important because this helped to achieve the necessary current value for the correct operation of the regenerative braking system. It is important to note the effects that the DC motor had on the EV system and the good performance obtained by the neural controller. Additionally, the proposed controller was compared with the PI controller, regarding reference tracking and robustness against parameter variations. The obtained results illustrated the effectiveness of the proposed control scheme for the AES trajectory tracking even in the presence of time-varying references and disturbances. The mean squared error helped to get a better idea of the improvement that the neural controller presented over a PI controller in this case. The measure of the error showed by far the effectiveness of NIOC even in the presence of disturbances or undesired signals. In addition, the charging and discharging of the AES supercapacitor during acceleration and deceleration was ensured, which helped to recover the wasted energy during braking and to participate in the MES's power budget during acceleration; moreover, it increases the lifetime of the battery bank. As a result, the charge duration of the MES battery bank was largely enhanced, and the electric vehicle's efficiency and operation were improved. Finally, it is necessary to mention that a real-time implementation is very important to consider; thus, the validation of the proposed controller will let us know its real effectiveness in terms of real driving performance. Moreover, new approaches for the inverse optimal and another neural controller such as the neural sliding mode control could be the simulation of a fully electric vehicle model system, where more important variables such as temperature conditions are considered, and the controllers are validated during typical driving conditions.

Author Contributions: Conceptualization, L.D.; methodology, J.A.R.-H. and L.D.; validation, E.N.S. and M.B.; formal analysis, M.A.R.C. and L.D.; investigation, J.A.R.-H., M.A.R.C. and L.D.; software, M.A.R.C. and L.D.; writing—original draft preparation, M.A.R.C. and L.D.; writing—review and editing, M.A.R.C., J.R, L.D., E.N.S. and M.B.; funding acquisition, M.A.R.C. All authors have read and agreed to the published version of the manuscript.

Funding: This research was funded by Consejo Nacional de Ciencia y Tecnología (México) (1085717).

Data Availability Statement: Not applicable.

Conflicts of Interest: The authors declare no conflict of interest.

References

1. Pavlović, T.; Mirjanić, D.; Mitića, I.; Stanković, A. The Impact of Electric Cars Use on the Environment. In *New Technologies, Development and Application II. NT 2019*; Karabegović, I., Ed.; Lecture Notes in Networks and Systems; Springer: Sarajevo, Bosnia and Herzegovina, 2019; Volume 76, pp. 541–548. [CrossRef]
2. Yoong, M.K.; Gan, Y.; Gan, G.; Leong, C.; Phuan, Z.; Cheah, B.; Chew, K. Studies of regenerative braking in electric vehicle. In Proceedings of the 2010 IEEE Conference on Sustainable Utilization and Development in Engineering and Technology, Petaling Jaya, Malaysia, 20–21 November 2010; pp. 40–45.
3. Tran, M.-K.; Bhatti, A.; Vrolik, R.; Wong, D.; Panchal., S.; Flowler, M.; Fraser, R. A Review of Range Extenders in Battery Electric. *World Electr. Veh. J.* **2021**, *12*, 54. [CrossRef]
4. Tie, S.F.; Tan, C.W. A review of energy sources and energy management system in electric vehicles. *Renew. Sustain. Energy Rev.* **2013**, *20*, 82–102. [CrossRef]
5. Villalobos, J.G.; Zamora, I.; Martín, J.S.; Asensio, F.; Aperribay, V. Plug-in electric vehicles in electric distribution networks: A review of smart charging approaches. *Renew. Sustain. Energy Rev.* **2014**, *38*, 717–731. [CrossRef]
6. Hannan, M.A.; Azidin, F.; Mohamed, A. Hybrid electric vehicles and their challenges: A review. *Renew. Sustain. Energy Rev.* **2014**, *29*, 135–150. [CrossRef]

7. Ortuzar, M.; Moreno, J.; Dixon, J. Ultracapacitor-Based Auxiliary Energy System for an Electric Vehicle: Implementation and Evaluation. *IEEE Trans. Ind. Electron.* **2007**, *54*, 2147–2156. [CrossRef]
8. Husain, I.; Ozpineci, B.; Sariful, M.I.; Gurpinar, E.; Su, G.; Yu, W.; Chowdhury, S.; Xue, L.; Rahman, D.; Sahu, R. Electric drive technology trends, challenges, and opportunities for future electric vehicles. *Proc. IEEE* **2021**, *109*, 1039–1059. [CrossRef]
9. Zhang, L.; Cai, X. Control strategy of regenerative braking system in electric vehicles. *Energy Procedia* **2018**, *152*, 496–501. [CrossRef]
10. Xie, J.; Cao, B.; Zhang, H.; Xu, D. Switched robust control of regenerative braking of electric vehicles. In Proceedings of the the 2010 IEEE International Conference on Information and Automation, Harbin, China, 20–23 June 2010; pp. 1609–1612. [CrossRef]
11. Xu, W.; Chen, H.; Zhao, H.; Ren, B. Torque optimization control for electric vehicles with four in-wheel motors equipped with regenerative braking system. *Mechatronics* **2019**, *57*, 95–108. [CrossRef]
12. Kiddee, K.; Keyoonwong, W.; Khan-Ngern, W. An HSC/battery energy storage system-based regenerative braking system control mechanism for battery electric vehicles. *IEEJ Trans. Electr. Electron. Eng.* **2019**, *14*, 457–466. [CrossRef]
13. Indragandhi, V.; Selvamathi, R.; Gunapriya, D.; Balagurunathan, B.; Suresh, G.; Chitra, A. An Efficient Regenerative Braking System Based on Battery-Ultracapacitor for Electric Vehicles. In Proceedings of the 2021 Innovations in Power and Advanced Computing Technologies (i-PACT), Kuala Lumpur, Malaysia, 27–29 November 2021.
14. Manríquez, E.Q.; Sanchez, E.N.; Toledo, M.E.A.; Muñoz, F. Neural control of an induction motor with regenerative braking as electric vehicle architecture. *Eng. Appl. Artif. Intell.* **2021**, *104*, 104275. [CrossRef]
15. Guo, J.; Xiaoping, J.; Guangyu, L. Performance Evaluation of an Anti-Lock Braking System for Electric Vehicles with a Fuzzy Sliding Mode Controller. *Energies* **2014**, *7*, 6459–6476. [CrossRef]
16. Li, X.; Xu, L.; Hua, J.; Li, J.; Ouyang, M. Regenerative braking control strategy for fuel cell hybrid vehicles using fuzzy logic. In Proceedings of the 2008 International Conference on Electrical Machines and Systems, Wuhan, China, 17–20 October 2008; pp. 2712–2716.
17. Rajendran, S.; Spurgeon, S.; Tsampardoukas, G.; Hampson, R. Intelligent Sliding Mode Scheme for Regenerative Braking Control. *IFAC-PapersOnLine* **2018**, *51*, 334–339. [CrossRef]
18. Wu, J.; Lu, Y. Decoupling and optimal control of multilevel buck DC-DC converters with inverse system theory. *IEEE Trans. Ind. Electron.* **2019**, *67*, 7861–7870. [CrossRef]
19. Manriquez, E.Q.; Sanchez, E.N.; Harley, R.G.; Li, S.; Felix, R.A. Neural inverse optimal control implementation for induction motors via rapid control prototyping. *IEEE Trans. Power Electron.* **2018**, *34*, 5981–5992. [CrossRef]
20. Cao, F.; Yang, T.; Li, Y.; Tong, S. Adaptive Neural Inverse Optimal Control for a Class of Strict Feedback Stochastic Nonlinear Systems. In Proceedings of the 2019 IEEE 8th Data Driven Control and Learning Systems Conference (DDCLS), Dali, China, 24–27 May 2019; pp. 432–436. [CrossRef]
21. Sanchez, E.N.; Alanis, A.Y.; Loukianov, A.G. *Discrete-Time High Order Neural Control: Trained with Kalman Filtering*; Springer Science & Business Media: Cham, Switzerland, 2008. [CrossRef]
22. Rios, Y.Y.; Garcia-Rodriguez, J.A.; Sanchez, E.N.; Alanis, A.Y.; Velázquez, E.R. Rapid Prototyping of Neuro-Fuzzy Inverse Optimal Control as Applied to T1DM Patients. In Proceedings of the 2018 IEEE Latin American Conference on Computational Intelligence (LA-CCI), Gudalajara, Mexico, 7–9 November 2018; pp. 1–5. [CrossRef]
23. Djilali, L.; Vega, C.J.; Sanchez, E.N.; Hernandez, J.A.R. Distributed Cooperative Neural Inverse Optimal Control of Microgrids for Island and Grid-Connected Operations. *IEEE Trans. Smart Grid* **2022**, *13*, 928–940. [CrossRef]
24. Franco, M.L.; Sanchez, E.N.; Alanis, A.Y.; Franco, C.L.; Daniel, N.A. Decentralized control for stabilization of nonlinear multi-agent systems using neural inverse optimal control. *Neurocomputing* **2015**, *168*, 81–91. [CrossRef]
25. Cao, J.; Cao, B.; Xu, P.; Bai, Z. Regenerative-Braking Sliding Mode Control of Electric Vehicle Based on Neural Network Identification. In Proceedings of the 2008 IEEE/ASME International Conference on Advanced Intelligent Mechatronics, Xi'an, China, 2–5 July 2008; pp. 1219–1224. [CrossRef]
26. Djilali, L.; Sanchez, E.N.; Ornelas-Tellez, F.; Avalos, A.; Belkheiri, M. Improving Microgrid Low-Voltage Ride-Through Capacity Using Neural Control. *IEEE Syst. J.* **2020**, *14*, 2825–2836. [CrossRef]
27. Alanis, A.Y.; Sanchez, E.N.; Loukianov, A.G. Discrete-time adaptive backstepping nonlinear control via high-order neural networks. *IEEE Trans. Neural Netw.* **2007**, *18*, 1185–1195. [CrossRef] [PubMed]
28. Sanchez, E.; Ornelas, F. *Discrete-Time Inverse Optimal Control for Nonlinear Systems*, 1st ed.; CRC Press: Boca Raton, FL, USA, 2013. [CrossRef]
29. Freeman, R.; Kokotovic, P.V. *Robust Nonlinear Control Design: State-Space and Lyapunov Techniques*; Springer Science & Business Media: Cham, Switzerland, 2008. [CrossRef]
30. Ruiz-Cruz, R.; Sanchez, E.; Loukianov, A.; Ruz-Hernandez, J. Real-time neural inverse optimal control for a wind generator. *IEEE Trans. Sustain. Energy* **2018**, *10*, 1172–1183. [CrossRef]
31. Rovithakis, G.A.; Chistodoulou, M.A. *Adaptive Control with Recurrent High-Order Neural Networks: Theory and Industrial Applications*; Springer Science & Business Media: Cham, Switzerland, 2012. [CrossRef]
32. Utkin, V.; Guldner, J.; Shi, J. *Sliding Mode Control in Electro-Mechanical Systems*; CRC Press: Boca Raton, FL, USA, 2017. [CrossRef]
33. Zohuri, B. *Scalar Wave Driven Energy Applications*; Springer: Cham, Switzerland, 2019. [CrossRef]